



On the connection between mode II and mode III effective thresholds in metals

Tomáš Vojtek, Stanislav Žák, Jaroslav Pokluda

Central European Institute of Technology (CEITEC), Brno University of Technology, Purkyňova 123, 612 00 Brno, Czech Republic

tomas.vojtek@ceitec.vutbr.cz, stanislav.zak@ceitec.vutbr.cz, pokluda@fme.vutbr.cz

ABSTRACT. Closure-free long cracks under the remote mode III loading grow in a more complicated way than those under the remote mode II. For bcc metals, a coplanar in-plane spreading of tongues driven by the local mode II loading components at crack-front asperities prevails while twisting of crack-front segments to mode I, often leading to factory-roof morphology, is typical for other materials. In bcc metals, therefore, the formulation of a quantitative relationship connecting effective thresholds in modes II and III demands to calculate the local mode II components of stress intensity factors at typical asperities of a crack front loaded in the remote mode III. Therefore, a numerical model of a serrated crack front was created and the results were compared with experimentally determined ratio of mode II and III effective thresholds for the ARMCO iron. Although the calculated crack-front roughness needs an experimental verification, the preliminary results indicate that the model can provide a quantitative explanation of the experimentally observed ratio of mode II and mode III effective thresholds in bcc metals.

KEYWORDS. Modes II and III; Effective threshold; Micromechanism; Finite element method; ARMCO iron.



Citation: Vojtek, T., Žák, S., Pokluda, J., On the connection between mode II and mode III effective thresholds in metals, *Frattura ed Integrità Strutturale*, 40 (2017) 245-251.

Received: 28.02.2017

Accepted: 03.05.2017

Published: 01.07.2017

Copyright: © 2017 This is an open access article under the terms of the CC-BY 4.0, which permits unrestricted use, distribution, and reproduction in any medium, provided the original author and source are credited.

INTRODUCTION

Despite the applied (remote) shear-mode II, III or II+III loading, the fronts of long cracks in metallic materials are, particularly in the small-scale yielding case, always loaded in a local mixed mode I+II+III due to their 3D microscopic tortuosity and frictionally induced mode I (e.g. [1], [2]). The contact of asperities in the crack wake (friction stress) induces a rather high crack tip shielding level which, as a rule, makes the extrinsic component of the resistance to the crack growth higher than the intrinsic one [3]. After a certain crack extension, such cracks start to deflect from the plane of the maximum shear stress to reduce the extrinsic resistance (the friction stress) by increasing the mode I loading component [4 – 9]. Consequently, the shear-mode cracks usually rather quickly become opening-mode cracks and the investigation of shear-mode crack-growth mechanisms and the related intrinsic resistance is very difficult. However, one can still experimentally uncover the crack growth mechanisms and the intrinsic resistance (effective thresholds) for

loading modes II and III by minimizing the extrinsic resistance by the preparation of fatigue precracks using cyclic compressive loading and subsequent annealing [10]. Such experiments revealed two basic types of closure-free propagation of mode II and mode III cracks in metallic materials [3]. First, the shear-mode propagation coplanar with precrack was observed for mode II loading in the case of bcc metals (e.g. ferritic steel or niobium) [11, 12]. In these materials, the dense set of slip planes in the bcc crystal lattice enabled creation and movement of dislocations in the slip planes lying sufficiently close to the plane of the maximum shear stress and thus possessing a high Schmid factor. The crack growth then proceeded along this plane in a nearly coplanar manner. The propagation of mode III cracks in the bcc metals was also found to be coplanar but the micromechanism revealed to be a spreading of in-plane tongues inclined by only very small angles to the macroscopic mode III crack front, thus driven by local mode II loading components [13]. These tongues mostly initiated on asperities (protrusions) of the microscopically tortuous crack fronts. The second (non-coplanar) type of crack growth was observed in materials with a low spatial density of slip systems (fcc) or with microstructural barriers for dislocation movement such as the pearlitic steel. In these materials, the fronts of the mode II cracks immediately deflected from the shear plane to experience a pure mode I loading whereas the mode III crack fronts locally twisted to create mode I segments which could lead to a formation of the factory-roof morphology. The growth mechanism in hcp materials represented a transition between the above mentioned two principal types [14, 15].

Thus, for the same specimen geometry and the same kind of shear-mode loading, different materials exhibit different crack paths. However, just a combination of local mode I and local mode II growth mechanisms is relevant for description of behaviour of most metallic materials [3, 12, 13] under all kinds of shear-modes (II, III and II+III). The classical criteria for mixed-mode crack propagation [16 – 18] do not take these differences into account and do not reflect the physical nature of the process. Such criteria cannot be reliably applied to mode II and mode III crack growth since there is no local mode III growth mechanism adequately efficient with respect to that of the mode II [19, 20]. The cracks grow under local mode I or II mechanisms instead [15, 21]. To apply the approach of local growth mechanism it is necessary to determine the local SIFs for the spatially oriented crack fronts. Such analysis was already done for remote mode II cracks [15]. The results led to a formulation of predictive relationship for the effective mode II threshold, which was verified by experimentally measured values. In the case of mode III cracks, however, the analysis is much more difficult due to the complicated mechanisms of local mode II crack advances or factory roof formation. Therefore, no quantitative expression for prediction of the effective mode III threshold was found hitherto.

The present paper addresses the problem of the prediction of effective mode III threshold for the ARMCO iron as a case study of materials with coplanar shear-mode crack propagation. For such materials, the 2D (in-plane) modelling of the tortuous crack geometry is sufficiently relevant and, therefore, the finite element analysis of the local mode II component for a crack with serrated (zig-zag) front loaded in the remote mode III was performed. The results are useful for expression of the ratio k_2/K_{III} of local mode II SIF to the global mode III SIF for a straight crack front, which can be compared with the experimentally measured ratio of effective thresholds $\Delta K_{II,eff,th}$ and $\Delta K_{III,eff,th}$.

MATERIAL AND EXPERIMENTS

Experimental data were evaluated for the ARMCO iron which is a nearly pure ferrite, as a representative of pure bcc metals. The mode III fatigue crack propagation experiment was performed using specimens cyclically loaded in torsion. The cylindrical specimens had a circumferential notch with the outer diameter $D = 25$ mm and the inner diameter $d = 12$ mm. A detailed description of the experimental arrangement can be found in [10].

The precracks were generated at the notch root by cyclic compressive loading [22 – 24] which resulted in an open precrack and avoided closure effects such as friction and contact of the fracture surfaces. After precracking the specimens were annealed in vacuum in order to eliminate the plastic zone in the vicinity of the crack tip and to avoid creation of an oxide layer. In this way, the effective (closure-free) mode III crack propagation threshold was measured. After applying $N = 10^5$ loading cycles with the cyclic stress ratio $R = 0.1$ at room temperature the experiments were stopped and the specimens were fractured by cyclic push-pull loading in mode I. The fracture surfaces were observed in the scanning electron microscope (SEM), where the crack length was measured.

NUMERICAL MODEL

To evaluate local stress intensity factors along the tortuous precrack front a finite element model [25] created with ANSYS finite element modeller was adapted. Because of the applied loading and the geometry of the specimen a full 3D model had to be used for the torsion specimen and one symmetry plane was used for the shear specimen.

Also, a submodelling procedure was employed to minimize the computational time.

The first stage model (global model) described deformation of whole specimen with smooth precrack front (no tortuosity) under respective loads. The second stage model (submodel) contained the tortuous precrack front. Its geometry was parameterized and defined by the main dimensions of the tortuosity (tooth height and length). A zig-zag shape of the precrack front was created by alternating key-points between maximal (R_{\max}) and minimal (R_{\min}) precrack front radii and by connecting these points to create the serrated crack front (see Fig. 1). A scripted code ensured that the number of modelled teeth was an integer (to avoid discontinuities at the crack front).

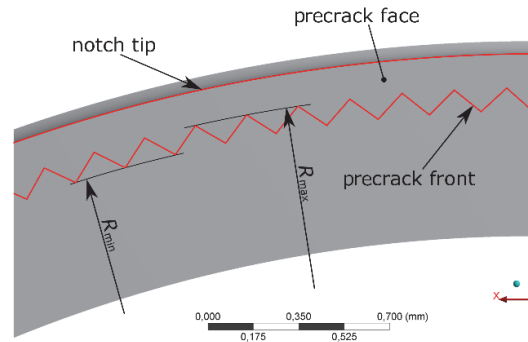


Figure 1: Scheme of the precrack emanating from the notch and possessing a serrated front.

Geometrical model was discretized by a very fine mesh of finite elements. ANSYS quadratic elements (SOLID186) were used and the rotational symmetry was employed to create a mostly uniform mesh. The model was adjusted to have 10 elements in the radial direction from the notch tip to the precrack front and 4 elements along each half-tooth at the precrack front.

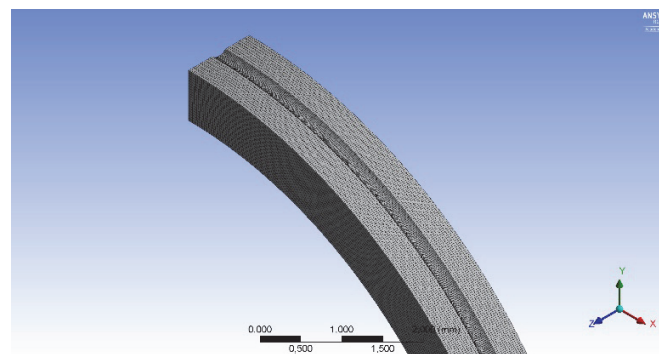


Figure 2: Submodel (finite element mesh).

This arrangement resulted in 9 nodes along each half-tooth. To evaluate the SIFs the ANSYS code used a domain integration around each evaluated point at the precrack front to compute the so-called interaction integral. Then the local SIFs were calculated from this integral [26] with respect to local coordinate systems. This calculation was performed for all nodes along the precrack front which provided 17 values of local SIFs (including one value for the conjoint node) along each precrack tooth.

RESULTS AND DISCUSSION

Local SIFs k_1 , k_2 and k_3 were evaluated for the remote mode III loaded crack with two crack geometries [27]. The first one was a smooth circular crack front and the second one was the serrated front (roughness asperities) characterized by the angle α .

The inclination of the crack front segments with respect to the remote shear stress resulted in a non-zero local mode II component. Significance of this component was assessed by the ratio of the local mode II SIF k_2 and the remote mode III SIF K_{III} determined for crack without ledges (asperities). This ratio was denoted r_{cal} and plotted in Fig. 4 for one half of

the asperity (see Fig. 3). The points at which the values were calculated are denoted by integers from 1 to 9 and they define the horizontal axis of Fig. 4. Only the values for points 2 to 8 are shown, since the extreme points 1 and 9 represent a discontinuity of the crack front and the corresponding SIFs are not well defined.

Ratios $r_{cal} = k_2/K_{III}$ were calculated as functions of different angles α in all nodes along the half tooth and plotted in Fig. 4. In this figure each data line corresponds to one angle α .

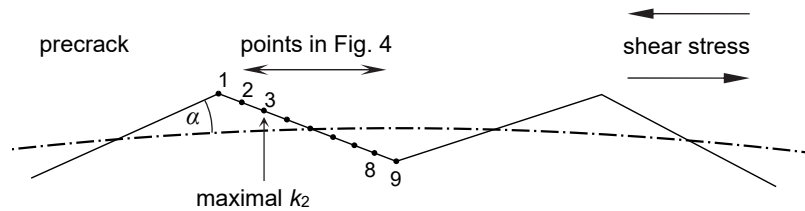


Figure 3: The detail of roughness asperities characterized by the angle α .

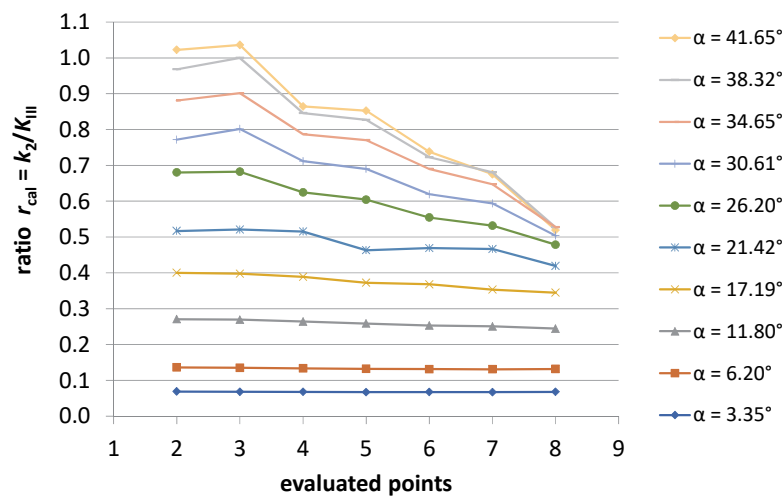


Figure 4: Results of r_{cal} for different asperity angles α in the range from 3.35° to 41.65° in points showed in Fig. 3.

Although the ratio r_{cal} is changing along the asperity, a useful dependence of the ratio r_{cal} on the asperity angle α can be still constructed from the computed curves in Fig. 4. Indeed, two special values of r_{cal} can be selected: the average value $r_{cal,av}$ (calculated from points 2 to 8) and the maximum value $r_{cal,max}$ (at the point 3) that is probably relevant for the first extension of local tongues at the threshold. Both $r_{cal,av}$ and $r_{cal,max}$ as functions of α are plotted in Fig. 5.

The SIF range ΔK_{III} measured at the mode III threshold under the presumption of a smooth circumferential crack front is equal to $\Delta K_{III,eff,th}$. Simultaneously, the local mode II component of the SIF range Δk_2 at the asperities (initiation sites of mode II tongues) should be equal to the measured $\Delta K_{II,eff,th}$. This means that the following formula must hold at the mode III threshold:

$$r_{cal} = \frac{k_2}{K_{III}} = \frac{\Delta k_2}{\Delta K_{III}} = \frac{\Delta K_{II,eff,th}}{\Delta K_{III,eff,th}} = r_{exp} \quad (1)$$

The agreement between theory and experiment could be tested by Eq. (1) since, for the ARMCO iron [10], the experimental ratio r_{exp} was obtained as

$$r_{exp} = \frac{\Delta K_{II,eff,th}}{\Delta K_{III,eff,th}} = \frac{1.5 \text{ MPa m}^{1/2}}{2.6 \text{ MPa m}^{1/2}} = 0.58 \quad (2)$$

The value $r_{exp} = 0.58$ was plotted in Fig. 5 as the horizontal dashed line and its intersection with the relevant curve $r_{cal,max}$ vs. α indicates that the characteristic angle α of the asperities at the precrack fronts in the ARMCO iron specimens should



be of 23° . This value must be, of course, verified by the measured linear roughness of these precrack fronts. Nevertheless, it seems to be plausible and sufficiently small to allow the local mode II mechanism operate at real micro-tortuous crack fronts without sharp protrusions.

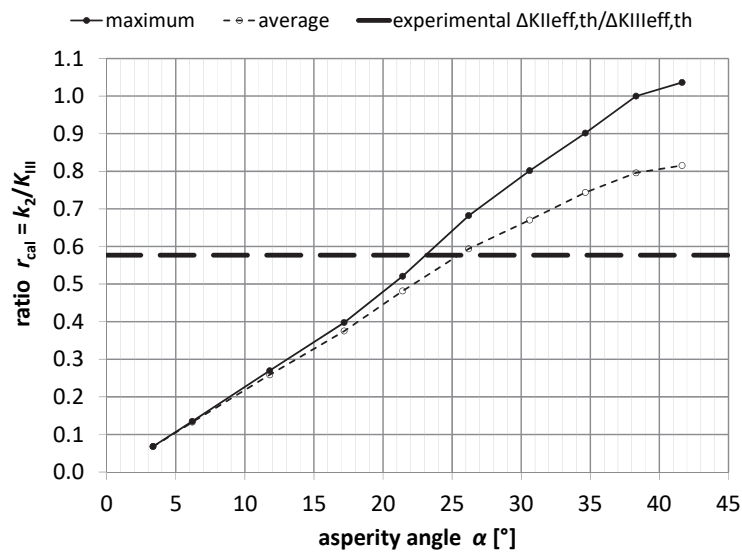


Figure 5: Dependences of $r_{cal,max}$ and $r_{cal,av}$ on the asperity angle α calculated for the respective points of the maximal value (stress concentration at point 3 in Fig. 3) and of the averaged value of the ratio r_{cal} along the half tooth (points 2 to 8). The horizontal dashed line represents the experimental ratio of effective thresholds $\Delta K_{IIeff,th} / \Delta K_{IIIeff,th}$.

The model of local mode I/II crack growth was already able to explain the existence of crystallographic facets oriented nearly parallel with the shear stress direction. It was also used to propose the formula for prediction of the intrinsic mode II threshold [15], which was found in a good agreement with experiments for many metallic materials. This study represents an important further step on the way to achieve an appropriate quantitative description of the effective mode III thresholds too. The results obtained by relatively complicated numerical calculations made to determine the local mode II SIFs of the serrated crack front seem to be very promising in terms of finding such a relationship.

CONCLUSION

This study represents an important step on the way to quantitatively describe the effective mode III thresholds in metallic materials with the bcc crystal lattice. In these materials, the micromechanism of propagation of mode III cracks was found to be a coplanar (in-plane) spreading of tongues driven by the local mode II loading component at asperities of micro-tortuous crack fronts. Since the in-plane 2D modelling of the tortuous crack geometry is sufficiently relevant here, the finite element analysis of the local mode II component for a precrack with serrated front loaded in the remote mode III was performed. Comparison of the calculated results with experimentally determined ratio of mode II and III effective thresholds revealed that, for the ARMCO iron as a case study, the characteristic angle α of the asperities (saw teeth) at the precrack front should be of 23° . Although this value must be verified by the measured linear roughness of the precrack fronts in the ARMCO specimens, it seems to be plausible and sufficiently small to allow the local mode II mechanism operate at real micro-tortuous crack fronts without any sharp protrusions. Thus, the result achieved is promising in terms of finding a physically justified formula for mode III effective thresholds in metallic materials with bcc lattice.

ACKNOWLEDGEMENTS

The authors acknowledge the financial support of this work by the Czech Science Foundation (GA CR) in the frame of the Projects No. 17-15716Y and No. 17-18566S, and by the Ministry of Education, Youth and Sports of the Czech Republic under the project CEITEC 2020 (LQ1601).



REFERENCES

- [1] Pokluda, J., Šandera, P., *Micromechanisms of Fracture and Fatigue. In a multiscale context*, London, UK: Springer; (2010).
- [2] Gross, T.S., Mendelsohn, D., Mode I stress intensity factors induced by fracture surface roughness under pure mode III loading: application to the effect of loading modes on stress corrosion crack growth, *Metal. Transactions*, 20A (1989) 1989–1999. DOI: 10.1007/BF02650285.
- [3] Pokluda, J., Pippan, R., Vojtek, T., Hohenwarther, A., Near-threshold Behaviour of Shear-mode Fatigue Cracks in Metallic Materials, *Fatigue Fract. Eng. Mater. Struct.*, 37 (2014) 232–254. DOI: 10.1111/ffe.12131.
- [4] Pinna, C., Doquet, V., The preferred fatigue crack propagation mode in a M250 maraging steel loaded in shear, *Fatigue Fract. Eng. Mater. Struct.*, 22 (1999) 173–183. DOI: 10.1046/j.1460-2695.1999.00161.x.
- [5] Doquet, V., Pommier, S., Fatigue crack growth under non-proportional mixed-mode loading in ferritic-pearlitic steel, *Fatigue Fract. Eng. Mater. Struct.*, 27 (2004) 1051–1060. DOI: 10.1111/j.1460-2695.2004.00817.x.
- [6] Doquet, V., Bertolino, G., Local approach to fatigue cracks bifurcation, *Int. J. Fract.*, 30 (2008) 942–950. DOI: j.ijfatigue.2007.06.001.
- [7] Doquet, V., Abadi, M., Bui, Q.H., Pons, A., Influence of the loading path on fatigue crack growth under mixed-mode loading, *Int. J. Fract.*, 159 (2009) 219–232. DOI: 10.1007/s10704-009-9396-6.
- [8] Murakami, Y., *Metal fatigue: effects of small defects and nonmetallic inclusions*, Amsterdam – Tokyo, Elsevier, (2002).
- [9] Gates, N., Fatemi, A., Friction and roughness induced closure effects on shear-mode crack growth and branching mechanisms, *Int. J. Fatigue*, 92 (2016) 442–458. DOI: 10.1016/j.ijfatigue.2016.01.023.
- [10] Vojtek, T., Pippan, R., Hohenwarther, A., Holáň, L., Pokluda, J., Near-threshold propagation of mode II and mode III fatigue cracks in ferrite and austenite, *Acta Mater.*, 61 (2013) 4625–4635. DOI: 10.1016/j.actamat.2013.04.033.
- [11] Vojtek, T., Pokluda, J., Hohenwarther, A., Pippan, R., Three-dimensional morphology of fracture surfaces generated by modes II and III fatigue loading in ferrite and austenite, *Eng. Fract. Mech.*, 108 (2013), 285–293. DOI: 10.1016/j.engfracmech.2013.02.022.
- [12] Vojtek, T., Pokluda, J., Hohenwarther, A., Pippan, R., Progress in Understanding of Intrinsic Resistance to Shear-mode Fatigue Crack Growth in Metallic Materials, *Int. J. Fatigue*, 89 (2016) 36–42. DOI: 10.1016/j.ijfatigue.2016.01.009.
- [13] Vojtek, T., Hohenwarther, A., Pippan, R., Pokluda, J., Experimental evidence of a common local mode II growth mechanism of fatigue cracks loaded in modes II, III and II + III in niobium and titanium, *Int. J. Fatigue*, 92 (2016) 470–477. DOI: 10.1016/j.ijfatigue.2016.02.042.
- [14] Vojtek, T., Pippan, R., Hohenwarther, A., Pokluda, J., Prediction of effective mode II fatigue crack growth threshold for metallic materials, *Eng. Fract. Mech.*, 174 (2017), 117–126. DOI: 10.1016/j.engfracmech.2016.11.024.
- [15] Vojtek, T., Pokluda, J., Experimental Investigation of Modes II and III Fatigue Crack Growth in Unalloyed Titanium, *Key Engineering Materials*, 592-593 (2014) 797–800. DOI: 10.4028/www.scientific.net/KEM.592-593.797.
- [16] Sih, G.C., Some basic problems in fracture mechanics and new concepts, *Eng. Fract. Mech.*, 5 (1973) 365–377.
- [17] Magill, M.A., An analysis of sustained mixed mode fatigue crack growth, *Eng. Fract. Mech.*, 56 (1997) 9–24. DOI: 10.1016/S0013-7944(96)00106-3.
- [18] Richard, H.A., Schramm, B., Schirmeisen, N.-H., Cracks on Mixed Mode loading – Theories, experiments, simulations, *Int. J. Fatigue*, 62 (2014) 93–103. DOI:10.1016/j.ijfatigue.2013.06.019.
- [19] Pokluda, J., Pippan, R., Can a pure mode III fatigue loading contribute to crack propagation in metallic materials?, *Fatigue Fract. Eng. Mater. Struct.*, 28 (2005) 179–185. DOI: 10.1111/j.1460-2695.2004.00843.x.
- [20] Doquet, V., Bui, Q.H., Bertolino, G., Merhy, E., Alves, L., 3D shear-mode fatigue crack growth in maraging steel and Ti-6Al-4V, *Int. J. Fract.*, 165 (2010) 61–76. DOI: 10.1007/s10704-010-9504-7.
- [21] Martins, R.F., Ferreira, L., Reis, L., Chambel, P., Fatigue crack growth under cyclic torsional loading, *Theor. Appl. Fract. Mech.*, 85A (2016) 56–66. DOI: 10.1016/j.tafmec.2016.08.016.
- [22] Suresh, S., Crack initiation in cyclic compression and its applications, *Eng. Fract. Mech.*, 21 (1985) 453–463. DOI: 10.1016/S0013-7944(85)80038-2.
- [23] Pippan, R., The growth of short cracks under cyclic compression, *Fatigue Fract. Eng. Mater. Struct.*, 9 (1987) 319–328. DOI: 10.1111/j.1460-2695.1987.tb00459.x.
- [24] Newman, J.C., Yamada, Y., Compression precracking methods to generate near-threshold fatigue-crack-growth-rate data, *Int. J. Fatigue*, 32 (2010) 879–885. DOI: 10.1016/j.ijfatigue.2009.02.030.



- [25] Žák, S., Horníková, J., Šandera, P., Pokluda, J., Verification of Linear Dependence of Plastic Zone Size on J-Integral for Mixed-Mode Loading, *Appl. Mech. Mater.*, 751 (2015) 15–20. DOI: 10.4028/www.scientific.net/AMM.751.15.
- [26] Ansys R16.2 help (manual), Ansys Inc., (2015).
- [27] Žák, S., Horníková, J., Šandera, P., Shear Mode Stress Intensity Factors for Serrated Crack Fronts, *Key Engineering Materials*, (2017), submitted to.